Mat. Res. Soc. Symp. Proc. Vol. 674 © 2001 Materials Research Society

Microscopic studies of fast phase transformations in GeSbTe films

Ralf Detemple, Inés Friedrich, Walter Njoroge,
Ingo Thomas, Volker Weidenhof,
Han-Willem Wöltgens, Stefan Ziegler, Matthias Wuttig
I. Physikalisches Institut der RWTH-Aachen, 52056 Aachen, Germany

ABSTRACT

Vital requirements for the future success of phase change media are high data transfer rates, i.e. fast processes to read, write and erase bits of information. The understanding and optimization of fast transformations is a considerable challenge since the processes only occur on a submicrometer length scale in actual bits. Hence both high temporal and spatial resolution is needed to unravel the essential details of the phase transformation. We employ a combination of fast optical measurements with microscopic analyses using atomic force microscopy (AFM) and transmission electron microscopy (TEM). The AFM measurements exploit the fact that the phase transformation from amorphous to crystalline is accompanied by a 6% volume reduction. This enables a measurement of the vertical and lateral speed of the phase transformation. Several examples will be presented showing the information gained by this combination of techniques.

INTRODUCTION

Rewritable optical data storage plays a key role for multimedia applications and could also be an interesting alternative for the mass storage of data. Phase change recording is a promising technique for the field of optical data storage since it is conceptionally compatible with present CD technologies. The principle behind phase change recording is the reversible transformation of small bits of the active layer between the stable crystalline and the metastable amorphous phase. Writing of bits corresponds to the formation of small amorphous marks in a crystalline matrix whereas the recrystallization of the amorphous areas leads to the erasure of the bit. Amorphization is achieved by locally melting the film using a focused laser beam. With rates between 10^9 and 10^{10} K/s the melt cools down and is trapped in the amorphous phase (called "quenching"). Heating the bits to a temperature between the glass transition and the melting temperature leads to its fast recrystallization. The amorphous phase can be distinguished from the crystalline phase by their optical properties. Therefore data can be read with a low power laser beam monitoring the local changes in reflectance.

One of the most important factors, which limits the applications for phase change-media like $Ge_2Sb_2Te_5$ [1], is a better understanding of the underlying microscopic processes, which occur during the phase transformation from amorphous to crystalline or vice versa. To unravel the processes occurring during the phase transformation, a high lateral and depth resolution is needed. We have established a combination of two techniques, atomic force microscopy and experiments with a static tester, which were used to investigate the amorphous and crystalline phases of written bits.

EXPERIMENTAL PROCEDURES

GeSbTe-alloys were deposited on glass or silicon substrates at room temperature by dc magnetron sputtering. The background pressure of the sputter system is 2×10^{-7}mbar. An argon pressure of 7.5×10^{-3}mbar and a power of 100 W was used to deposit the films. The resulting growth rate was determined to 0.5 nm/s.

X-ray reflectometry (XRR) measurements were performed to determine the thickness, roughness and the density while X-ray diffraction (XRD) measurements were used to determine the structure of the films. These measurements were carried out using a Philips X'pert MRD system. All measurements were performed at room temperature.

The bits were written with a static tester. A GaAlAs-laser diode with a wavelength of 830 nm driven by a pulse generator serves as a light source. The light is coupled into an objective with a numerical aperture of 0.9 and is focused onto the phase change material deposited onto glass. After the laser-induced modification of a certain region the sample can be moved with a piezo scan stage with nanometer precision. This allows us to write bit arrays in a region of 60×60 μm^2. The light reflected from the phase change material is monitored by a photo detector.

AFM measurements were performed with a Dimension 3100, which reveals the surface topography of the bits. The lateral resolution is limited by the curvature of the tip, which is around 10 nm.

RESULTS

AMORPHIZATION

XRR measurements were carried out to determine the change in density with annealing temperature. The density of the analysed sample was derived from the position of the total reflection edge Θ_c according to the formula

$$\rho = \left(\frac{\Theta_c}{\lambda}\right)^2 \frac{A\pi}{N_a r_0 (f_0 + f')} \qquad (1)$$

, where N_A is Avogadro's constant, r_0 is the Bohr radius, λ is the wavelength of x-rays, A is the atomic mass and (f_0+f') are the atomic form factors [2].

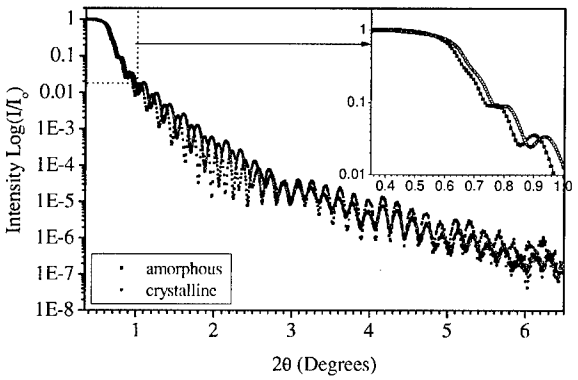

Figure 1: XRR spectra of an 80 nm thick $Ge_2Sb_2Te_5$ layer before (solid squares) and after (open circles) crystallization. The inset shows the shift of the total reflectivity edge, which was used to determine the density.

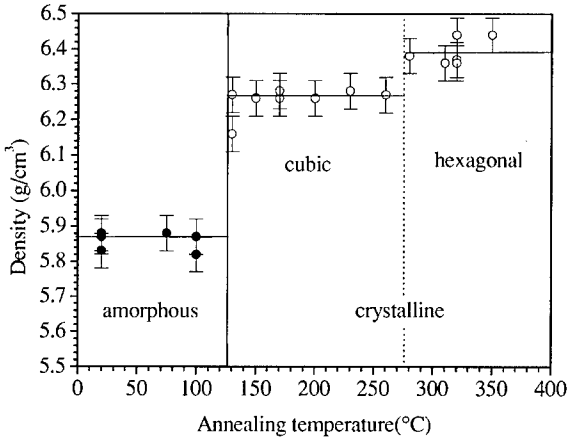

Figure 2: Density of $Ge_2Sb_2Te_5$ as a function of annealing temperature. The samples were annealed in an oven for 10 minutes. Above 130° C the rock salt structure (cubic phase) appears, at even higher temperature of 275° C the hexagonal phase is found.

The thickness of the as deposited amorphous and the crystalline sample was determined from simulations of the experimental spectra [3]. Typical spectra are shown in figure 1, where two measurements for the as deposited and crystalline cubic phase are compared. The calculated density is plotted in figure 2, which shows clearly three regimes of increasing density. The density of the amorphous phase is constant up to 130° C. Above this temperature, the rock salt

structure is formed. This phase transformation is accompanied by a density change of 6.8 %. The transformation to the hexagonal phase occurs if the temperature rises to values above 275° C, where a density change of 8.9 % with respect to the amorphous phase is found.

XRR measurements are, as mentioned above, performed on macroscopic samples annealed for 10 minutes in an oven. Nevertheless we can make use of the information displayed in figure 2 to understand the change in local topography created by a focussed laser pulse (figure 3). Amorphization in a crystalline matrix with cubic structure should lead to 6.8 % increase in thickness. For a film with a thickness of 80 nm this corresponds to a height change of about 5 nm. This is indeed what is observed by AFM. This height change enables us to track the lateral and depth growth. The density-difference between both phases and the measured height change (denoted as Δz in figure 4) was used to calculate the amorphous fraction of the bit. For this analysis we have subtracted the height change caused by delamination which is clearly visible in the outer halo. The remaining height change is attributed to the density change upon amorphization. Using a linear interpolation between a completely crystalline (thickness d) and an amorphous one (thickness $d \times \rho_c / \rho_a$) results in a relationship for the amorphous fraction χ:

$$\chi = \frac{\Delta z}{d\left(\frac{\rho_c}{\rho_a} - 1\right)} \qquad (2)$$

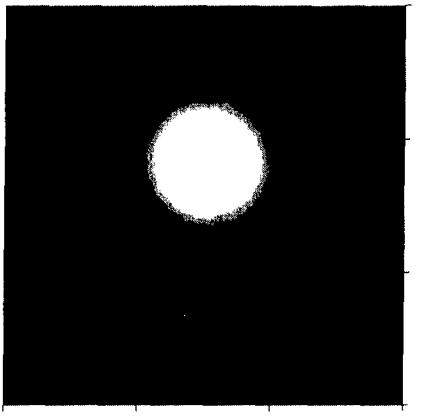

Figure 3: An AFM image of an amorphous bit in a crystalline environment. Only the inner white region consists of amorphous material, whereas the outer halo contains crystalline material. The halo is caused by a local stress relief which leads to a film delamination.

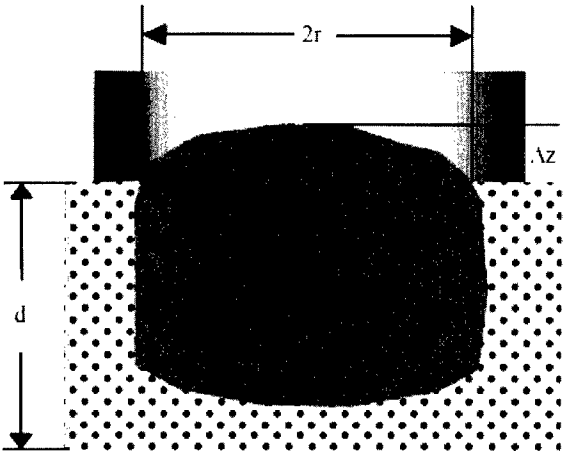

Figure 4: Schematic drawing of an amorphous bit. The total reflected power constitutes of an amorphous inner part and a crystalline surrounding area. Due to the gaussian form of the beam, both parts have to be weighted accordingly. The inner part is weighted with the factor *f*, which leads to an effective reflectivity $f \cdot R_\chi$. The surrounding surface has an effective reflectivity of $(1-f) \cdot R_c$ due to the crystalline phase. This method is used to calculate the optical reflectivity from AFM data. See text for details.

The simplest model, which can be used, describes the relation between reflectance and amorphous fraction is a linear relationship. More sophisticated models, including a depth dependent degree of amorphisation, will not lead to a better fit to the data. Defining the reflectivity as a linear function of the amorphous fraction, the reflectivity of the amorphized surface can be calculated:

$$R_\chi = R_c + \chi(R_a - R_c) \qquad (3)$$

Until now, only the reflection of the amorphous bit has been taken into account. The crystalline surrounding also contributes to the total reflected intensity. Furthermore, the gaussian form of the beam is taken into account by weighting both contributions. The fraction of the laser beam, which illuminates the inner region, is denoted as *f*.

$$f = 1 - \exp\left(-2(r/r_0)^2\right) \qquad (4)$$

where r is the bit radius and r_0 is the gaussian radius. Compiling all informations gives the total reflectivity:

$$R = f \cdot R_\chi + (1-f) \cdot R_c \qquad (5)$$

These theoretical reflectivities are compared with experimental data measured by the static tester in figure 5 [4]. A general agreement between the calculated values using AFM data and the reflectivity measured by the static tester has been found, which shows that from the AFM data we can determine the essentials of the process. Nevertheless the experimental data points still show a deviation from the theoretical values, which has two reasons. The curvature radius of the AFM tip is about 10 nm. In the worst case, this leads to an error of about 6% in the determination of the lateral size of the bit. The second source for deviations is the error in density, which was used to calculate the amorphous fraction χ. A third possible source for deviations, that can not be quantified, is the optical difference between the as deposited and the quenced amorphous phase.. The optical constants and the density used for the calculations were measured using as deposited samples. Since we have not observed any density change upon annealing up to the crystallization temperature, we believe that the density of the amorphous phase is almost identical for the as deposited and the laser quenched phase. The agreement shown in figure 5 proves, however, that AFM and static tester experiments give consistent results, despite the shortcomings mentioned above.

To identify the processes, which limit the speed of amorphization, the growth of amorphous bits has been decomposed into the lateral and vertical dimensions. Assuming a sharp boundary between the crystalline and amorphous phase, the vertical growth is given by the depth of the boundary:

$$d_{\text{int}} = \chi \cdot d_{cr} = \frac{\Delta z}{\left(\frac{\rho_c}{\rho_a}\right) - 1} \qquad (6)$$

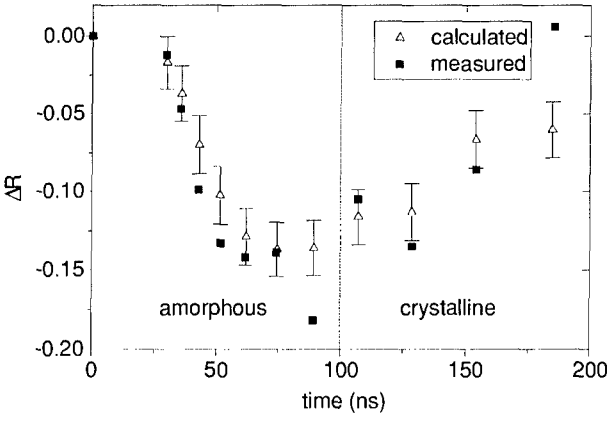

Figure 5: Comparison of experimental and theoretical reflectivity. For pulses shorter than 100 ns amorphization takes place. When the pulse length increases above this limit, melt-crystallization occurs.

Figure 6a shows the evolution of reflectivity measured by the static tester. The lateral size and the depth of the boundary in vertical direction are depicted in 6b and 6c as a function of pulse duration. The derivatives with respect to time show a strong correlation between the optical signal and the vertical growth speed. The process of amorphization is therefore mainly limited by the vertical growth speed, which reaches values up to 1 m/s. This can be explained by the gaussian beam profile, because the inner amorphous mark contributes the main fraction to the optical signal. The lateral growth of the bit has only a small impact on the readout signal, since the outer regions are only illuminated by a small fraction of the total laser intensity [5].

From the discussion presented above we can conclude that amorphization should be faster for thinner films. Therefore films with a thickness of 5 and 80 nm were compared. To determine the shortest time for successful amorphization, the power necessary to write an amorphous bit was varied and is visualized in figure 7. The reflectivity change as a function of pulse length (x-axis) and pulse power (y-axis) is color coded. If the laser power is low and the pulse duration too short, no phase change will be induced and the corresponding reflectivity change is close to zero (region I). With a laser power of about 5 mW, amorphization starts. In this region II, the illuminated area is molten and afterwards quenches into the amorphous phase. For a successful amorphization, a high temperature gradient is required to cool down the molten phase ($10^9 - 10^{10}$ K/s). When the volume around the molten bit gets warmer due to longer pulses (region III), the temperature gradient is too small and melt-crystallization takes place. For longer pulses and higher laser powers, ablation and loss of material occurs (region IV). The result of this experiment proves a faster amorphization for a 5 nm thin film. For example, when the 5 nm thick film needs 10 ns to amorphize at 20 mW, the 80 nm film needs 30 ns.

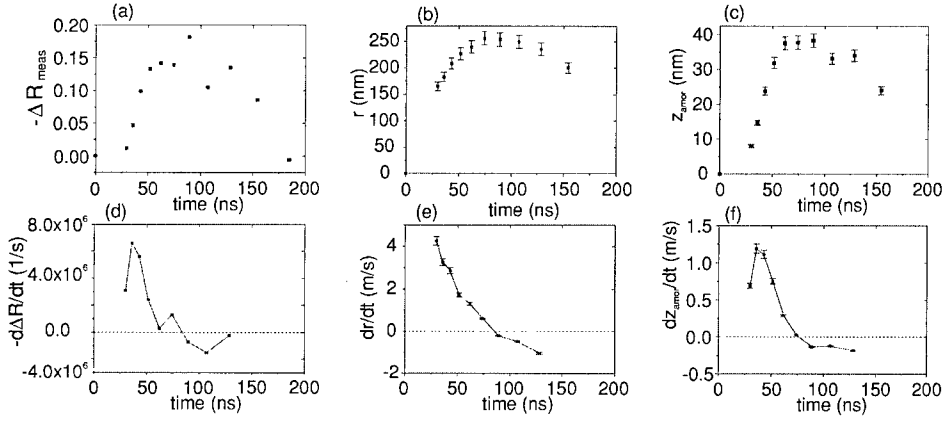

Figure 6: The upper row shows the evolution of the reflectivity change and the bit topography upon pulse length. The time derivatives of these data were calculated and presented in the bottom row. The change of reflectivity measured with the static tester is shown in the left column, while the lateral bit growth and the height change can be found on the right hand side. The change in reflectivity (6d) is dominated by the vertical growth (6f). The vertical growth speed (right bottom diagram) of about 1 m/s limits the maximum speed of amorphization.

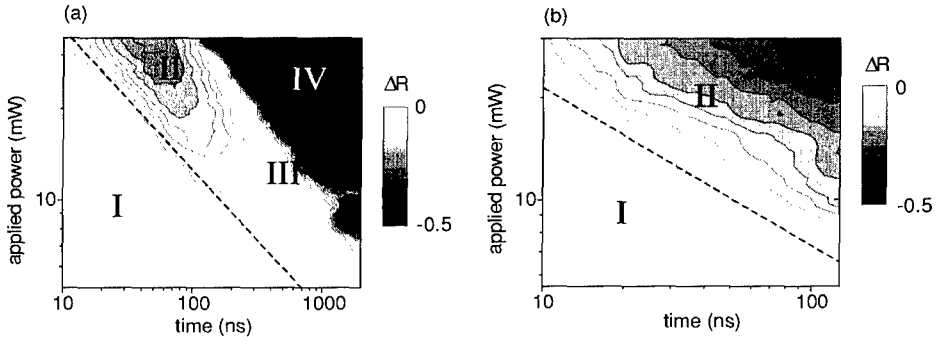

Figure 7: The influence of film thickness upon the pulse length necessary to amorphize is shown here for 80 nm (left) and 5 nm (right) films. Amorphization in 10 ns for thick samples can be achieved, if the laser power will be increased above 40 mW. Lower laser powers are sufficient for the thin sample (right picture), where a successful amorphization takes place for 20 mW in 10 ns.

CRYSTALLIZATION

To erase the written bits, they must be crystallized. Figure 8 shows the influence of the phase of the material surrounding the crystallized bit upon the pulse duration and pulse power necessary to crystallize.

In the left diagram of figure 8, an amorphous environment for the crystallization was chosen. The corresponding power-time-effect diagram shows a minimum time for crystallization of around 100 ns, which limits the crystallization process under these circumstances. This time of 100 ns is identified as the incubation time [6,7], which is needed to reach an equilibrium distribution of subcritical nuclei.

The minimum time to crystallize can be reduced by one order of magnitude if a crystalline environment is chosen, which is demonstrated in figure 8, right diagram. In contrast to prior shown PTE-diagrams, two pulses were used for every data point: First a pulse with fixed parameters to write a bit (amorphize the illuminated region), followed by a pulse with varying pulse power and duration. The respective change in reflectivity from the state before the first pulse and after the second one was measured. Region II marks the parameters for successful recrystallization, which starts at 10 ns. A second amorphization is also possible, as seen in region III. The physics related to a further increase in time is similar to amorphization, where melt-crystallization is observed.

This fast recrystallization is attributed to one of the two different mechanisms of recrystallization: Either small crystalline nuclei which are incorporated inside the amorphous material can start the recrystallization or it is started from the surrounding rim [10]. A differentiation can be made by measuring the recrystallized fraction ε after the second pulse as a function of the diameter of the initial, amorphous bit where ε is defined as

$$\varepsilon = 1 - \frac{R_{rec} - R_i}{R_i - R_a} \qquad (7)$$

R_i is the initial reflectivity, R_a the reflectivity after the amorphization pulse and R_{rec} the reflectivity after recrystallization pulse. R_{rec} is the weighted sum of the reflectivity of the recrystallized area and the remaining amorphous part. In the presence of small nuclei the recrystallization starts homogenously distributed throughout the amorphous part. Hence there is

no correlation between ε and the bit diameter. On the contrary, if the recrystallization starts from the rim, the recrystallization efficiency depends on the bit diameter. Regarding equation (7) we then expect a decrease in ε with bit diameter. This experiment was carried out with two different materials, $Ge_2Sb_2Te_5$ and $Ge_4Sb_1Te_5$ (figure 9). In the case of $Ge_2Sb_2Te_5$ there is no dependency between ε and bit diameter and thus small crystalline nuclei have to be present in the amorphous phase. However, in the case of $Ge_4Sb_1Te_5$ ε decreases with bit diameter and thus recrystallization has to start from the crystalline rim.

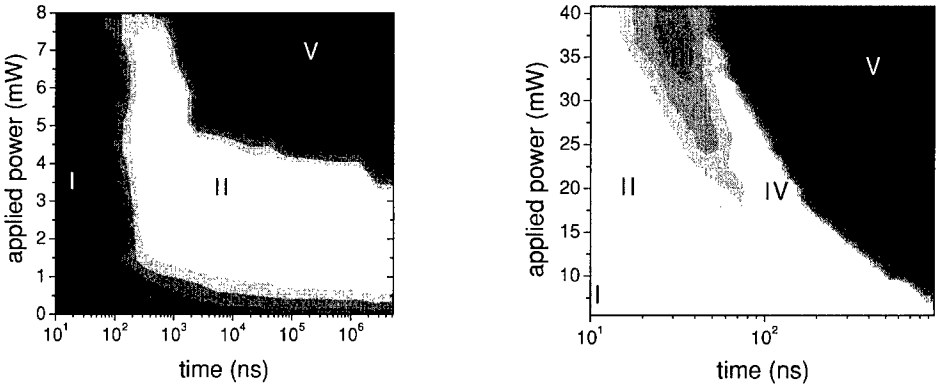

Figure 8: The influence of the environment surrounding the bits can be seen from these two power-time-effect diagrams. The diagram on the left hand side shows the effect of crystallization in an amorphous environment. Important is the minimum time for crystallization of 100 ns (region II). Using a crystalline environment considerably reduces this time limit, a successful crystallization (region II) is possible for pulse lengths of about 10 ns. Here two pulses were used: first one for amorphization (writing the bit) with constant parameters. The second pulse was varied in power and duration. If the second laser pulse is short and intense, amorphization can take place (region III). Like in figure 7, melt-crystallization can be observed for longer pulses, denoted as region IV.

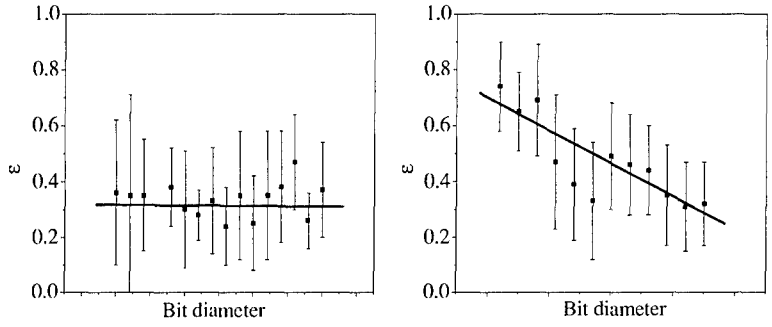

Figure 9: Recrystallized fraction of recrystallized bits as function of bit diameter. The left diagram corresponds to the material $Ge_2Sb_2Te_5$, which starts to recrystallize from small nuclei inside the amorphous material. The material $Ge_4Sb_1Te_5$ is shown on the right hand side. A shrinking remaining fraction indicates a crystallization, that starts from the rim.

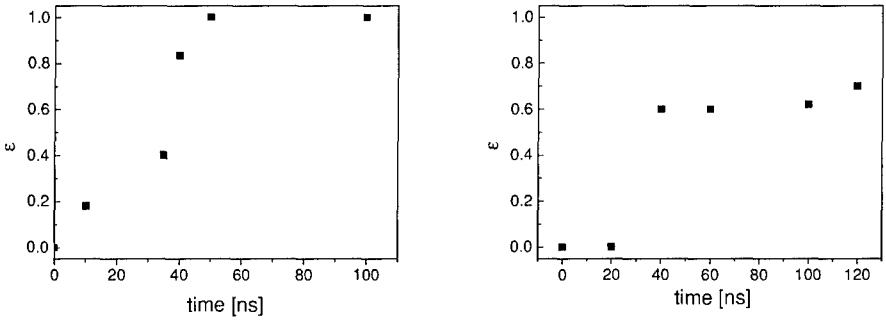

Figure 10: Erasure of amorphous bits in different crystallographic environments. Left: a cubic structure of the rim leads to a perfect erasure, which is identified by an epsilon of one. This state of the bit is reached after 50 ns. If a hexagonal structure is present, epsilon will not reach one, even after 120 ns. This is due to the phase transformation of the amorphous bit into the rock salt structure, which has a different reflectivity than the surrounding hexagonal phase.

We conclude, that the recrystallization starts for $Ge_2Sb_2Te_5$ at small crystallites. Until now it is not clear, what the structure of these nuclei is. To determine this microstructure, experiments with different macroscopically crystallized samples were carried out: a) cubic rock salt structure and b) hexagonal phase. The crystallized fraction ε as function of pulse duration of the recrystallization pulse is shown in figure 10. The erased bits, grown in an environment with cubic phase, were completely erased. This is indicated by the saturation level of epsilon = 1 for times longer than 50 ns. If the environment consists of the hexagonal crystal structure, also a saturation is reached, but now at a level of 0.6. This can be explained by the different optical properties of

both crystalline phases: The recrystallized volume will always consist of the cubic phase, so no difference between the initial and the final phase occurs (ε=1). In case b), the initial phase and final phase are different in respect to their crystal structure and also their optical properties (ε=0.6). The formation of the cubic phase for these nuclei can be explained by the shorter diffusion path needed to create the cubic in contrary to the more complex hexagonal phase. This is in good agreement to macroscopic experiments [11].

INFLUENCE OF A DIELECTRIC LAYER UPON AMORPHIZATION

In data storage applications, the active layer is sandwiched by dielectric layers. Hence, phase change materials on glass were covered with a 30 nm thick protective layer of $ZnS:SiO_2$ to study the effect of capping layers on the power-time-effect diagrams. For long pulses and high powers the formation of large bubbles of considerable height was observed, which were detected by AFM (figure 11) [9]. Such 125 nm high bubbles could be a major problem for near-field recording techniques. Argon which is incorporated during magnetron sputtering process is the most probable candidate responsible for these bubble formations. With Rutherford Backscattering it was shown that up to 0.8 atomic % argon is incorporated into the film during deposition. While the amorphization takes place, the temperature is larger than the melting temperature of the phase change material. In this liquid phase the argon gas will thermally expand and thus exert a pressure on the dielectric layer causing dome formation. Applying the equation of ideal gases at the melting temperature of the phase change material should give rise to a pressure of 5-7 MPa inside the bubbles. However, from surface curvature and surface energy we obtained a pressure

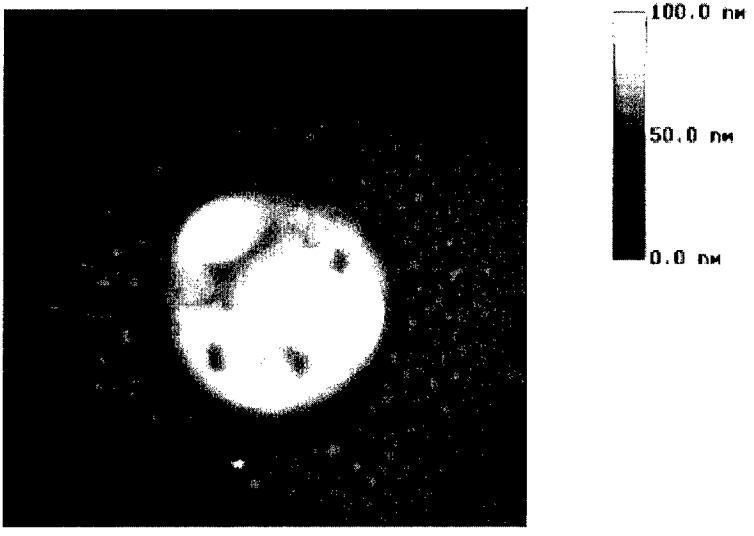

FIGURE 11: Amorphisation of $Ge_2Sb_2Te_5$ covered with 30 nm thin $ZnS:SiO_2$ with high laser powers leads to the formation of bubbles. These bubbles can grow up to 300 nm. The origin is the thermal expansion of the incorporated argon, deposited by the magnetron sputtering process.

of 12 MPa, which is from the same order as the value mentioned before. Combining these values with geometry a Young's Modulus of 35 – 50 MPa for the dielectric cover layer is calculated. This value is in good agreement to literature data [8], and hence proves that the incorporated argon is acting as the origin for the bubbles. Other sources for the volume change such as the expansion of the phase change material can be neglected. While Ar leads to a 40% volume expansion, the changes in volume due to the phase transformation is at most 9% (assuming a hexagonal reference phase).

CONCLUSIONS

We have examined the process of amorphization and crystallization in $Ge_2Sb_2Te_5$ to unravel the microscopic transformation mechanisms. The result of a maximum growth speed of 1 m/s leads to a thickness dependent minimum amorphization time. No kinetic superheating for times longer than 10 ns was observed. Fast erasure of amorphized bits within 10 ns is only possible in a crystalline environment, where two types of recrystallization, i.e. starting from small subcritical nuclei or from the rim, were identified for different stoichiometries of the alloys. The recrystallized bits always have the cubic structure, independent of the surrounding environment. A capping layer on top of the phase change material was lifted by thermal expansion of incorporated argon.

ACKNOWLEDGEMENTS

Financial support by the Fonds der Chemischen Industrie is gratefully acknowledged.

REFERENCES

1. M. Libera and M. Chen, MRS Bull. **15**, 40 (1990)
2. D.K.G. de Boer, Glancing-Incidence X-ray Fluorescence of layered materials, Phys. Rev. B 44 (1991) 498.
3. W. K. Njoroge, (unpublished)
4. V. Weidenhof et al., J. Appl. Phys. **88** (2), 657 (2000)
5. V. Weidenhof et al., J. Appl. Phys. **86** (10), 5879 (1999)
6. J. W. Christian, The Theory of Transformations in Metals and Alloys, Pergamon, New York (1965)
7. S. Nagpal and P.K. Bhatnagar, Phys. Stat. Sol. **161**, 59 (1997)
8. H. Ebert, Physikalisches Taschenbuch, Vieweg. Seite 260.
9. I. Thomas, Charakterisierung und Optimierung der Phasenumwandlungskinetik in GeSbTe-Legierungen, Diploma thesis, RWTH Aachen (2000)
10. J. H. Coombs et al. J. Appl. Phys. **78** (1995), 4918
11. I. Friedrich et al., J. Appl. Phys. **87** (9), 4130 (2000).